A Well-balanced Gas-Kinetic Scheme for the Shallow Water Equations with Source Terms

Kun Xu*
Department of Mathematics, Hong Kong University of Science and Technology, Clear Water Bay, Kowloon, Hong Kong

Abstract

This paper is about the extension of the gas-kinetic BGK scheme to the shallow water equations with source terms. In this approach, the particle velocity change due to the gravitational force and wary river bottom is implemented explicitly in the flux evaluation. The current scheme is a well balanced method, which presents accurate and robust results in both steady and unsteady flow simulations.

1 Introduction

In recent years, the study of the hyperbolic system with source terms has attracted much attention in the CFD community. One of the main reasons is that there exist wide engineering applications. For example, the Saint-Venant equations are widely used in ocean and hydraulic engineering to describe bore wave propagation, hydraulic jump, and open channel flow, among others. Many numerical schemes have been developed in the past decades for the above equations, see [2, 3, 6, 7, 9, 11, 12, 15, 18] and references therein.

The shallow water equations in 1-D case can be written as

$$W_t + F(W)_x = S, \tag{1.1}$$

where $W = (h, hU)^T$ is the vector of flow variables and $F(W) = (hU, hU^2 + \frac{1}{2}Gh^2)^T$ is the corresponding flux. In the above equations, h is the water depth and U is the water velocity. The source term has the form $S(W) = (0, -hGB'(x))^T$, which accounts for the effect from the gravitational force and wary river bottom on the fluid motion, and $B(x)$ is the shape of the bed profile. If we integrate the above equation against dx in a spatial element j from $x_{j-1/2}$ to $x_{j+1/2}$, and dt in a time interval from t^n to t^{n+1},

$$\int_{t^n}^{t^{n+1}} \int_{x_{j-1/2}}^{x_{j+1/2}} (W_t + F(W)_x) dx dt = \int_{t^n}^{t^{n+1}} \int_{x_{j-1/2}}^{x_{j+1/2}} S(W) dx dt,$$

*Email:makxu@uxmail.ust.hk, fax: (852)2358-1643, tel: (852)2358-7433.

we get

$$W_j^{n+1} - W_j^n = \frac{1}{\Delta x}\int_{t^n}^{t^{n+1}} \left(F_{j-1/2}(t) - F_{j+1/2}(t)\right) dt + \frac{1}{\Delta x}\int_{x_{j-1/2}}^{x_{j+1/2}} \int_{t^n}^{t^{n+1}} S(W) dx dt, \tag{1.2}$$

where $\Delta x = x_{j+1/2} - x_{j-1/2}$ is the cell size and W_j the average value of W in cell j, *i.e.*,

$$W_j = \frac{1}{\Delta x}\int_{x_{j-1/2}}^{x_{j+1/2}} W dx.$$

The above equation is an integral form of Eq.(1.1), which is exact and equivalent to Eq.(1.1). Physically, Eq.(1.2) reflects the following fact. The second term on the right hand side describes the gravitational effect on a fluid element moving from one place to another place **within** the same cell due to the non-smoothness of the river bottom. If the fluid element passes **through** the cell interface, its contribution is included in the first term on the right hand side of Eq.(1.2). Since the fluid particle should have no idea about the location of the cell interface, the non-smoothness of the river bottom and the gravitational force will equally take effect on any fluid element moving inside the same cell or passing through the cell interface. Therefore, a physical flux function in the above equation should include the source term influence too, such as the fluid acceleration or deceleration due to wary river bottom when going through the cell boundary. This is one of the main points we would like to address in the current paper.

Since different shapes of the river bottom have different dynamical influence on the fluid motion, in order to get an accurate solution based on Eq.(1.2) for the shallow water equations, we need to discretize the river bottom $B(x)$ first. For a first order approximation, the river bottom can be approximated as flat inside each cell, see Fig.(1), Eq.(1.2) becomes

$$W_j^{n+1} - W_j^n = \frac{1}{\Delta x}\int_{t^n}^{t^{n+1}} \left(F_{j-1/2}(t) - F_{j+1/2}(t)\right) dt. \tag{1.3}$$

The absence of the explicit source term in the above equation is due to the fact that $B'(x) = 0$ inside each cell. But, the flux in the above equations should be based not only on the flow variables W_j and W_{j+1}, but also on the bottom height jump from B_j to B_{j+1}. A Riemann solution based on the above initial condition has been obtained by a few authors [12, 1], see [8] also. Similar idea has been applied to other equations with different source terms [10]. Under the condition in Fig.(1), due to the bottom jump the momentum flux will not be continuous at the cell interface. In other words, the momentum lost in cell j at $x_{j+1/2}$ is not equal to the momentum received in cell $j+1$. The reason is that when the fluid passes through the cell interface, it has to overcome the gravitational barrier, where the kinetic and potential energy exchange takes place. Under the assumption of stationary step transition (SST) at the cell interface, there are about 20 cases of different wave patterns for the exact Riemann problem, and the solution itself can be hardly used in any practical flow applications [1]. On the contrary, in hydraulics engineering an empirical local head loss due to sudden channel geometry change is used to simulate the momentum flux discontinuity [5].

Since we have the freedom to choose the location of cell interface, an alternative choice is to shift the cell interface by half cell size, see Fig.(2). Note that the flow variables are based on the cell average and must be inside each cell. In this case, Eq.(1.2) becomes

$$W_j^{n+1} - W_j^n = \frac{1}{\Delta x}\int_{t^n}^{t^{n+1}} \left(F_{j-1/2}(t) - F_{j+1/2}(t)\right) dt + \frac{1}{\Delta x}\int_{x_{j-1/2}}^{x_{j+1/2}} \int_{t^n}^{t^{n+1}} S(W) dx dt.$$

Even though the above equation looks the same as Eq.(1.2), but they have contain different physical meanings. In the above equation, the flux evaluation can ignore the source term effect because of the zero slope of $B(x)$ around a cell interface, but the integration of the source term inside each cell becomes complicated due to the river bed jump. A solution which accounts for the source term inside each cell is obtained by LeVeque using quasi-steady approximation [11], which is similar to SST approximation. The scheme gives excellent results in the quasi-steady sound wave propagation cases, which may be difficult for most other well-balanced schemes in the literature when 100 or less grid points are used. But due to the quasi-steady approximation, LeVeque's scheme may have difficulties in the application to the unsteady flow with shock waves directly.

For a second order approximation of the river bottom, the bed shape can be approximated as a linear function inside each cell, see Fig.(3). As a special case, in order to develop a well balanced scheme, which is defined as a scheme to keep the solution $U = 0, h + B =$ constant exactly, see Fig.(4), the flux and source term have to be precisely matched,

$$\frac{1}{\Delta x}\int_{t^n}^{t^{n+1}} \left(F_{j-1/2}(t) - F_{j+1/2}(t)\right) dt = -\frac{1}{\Delta x}\int_{x_{j-1/2}}^{x_{j+1/2}} \int_{t^n}^{t^{n+1}} S_j(W) dx dt. \tag{1.4}$$

Many well balanced schemes have been designed based on the above equation. For example, when an upwinding scheme is used for the flux evaluation, a common way to keep the above equality is to approximate the source term, such as splitting it according to different wave modeling in the flux function, see [9, 3, 7] and references therein. It is true that Eq.(1.4) needs to be satisfied for a well balanced scheme, but the scheme designed from the satisfaction of the above equation may not be accurate and robust in other flow situations.

Recently, Zhou et. al. developed a robust and well balanced scheme based on the HLL Riemann solver and the surface gradient method (SGM) for initial data interpolation [18]. The merit of their approach is that their initial reconstruction is based on $h + B$ instead of h. Therefore, the equilibrium initial data $U = 0$ and $h + B =$ constant can be precisely kept after reconstruction. For example, in the case of Fig.(4), the water surface will keep flat after data reconstruction and the only flux contribution instantaneously at each cell interface is the pressure term $Gh_{j+1/2}^2/2$, which can be used to balance the source term effect exactly inside each cell,

$$\frac{1}{2}G(h_{j-1/2}^2 - h_{j+1/2}^2) = Gh_j(B_{j+1/2} - B_{j-1/2}). \tag{1.5}$$

So the equality in Eq.(1.4) holds. Even for the 2nd-order SGM with the implementation of the Hancock technique, due to the **independent time evolution** for the left and right states at a cell interface the fluid distribution at a middle time step $t^{n+1/2}$ can still keep the distribution profile in Fig.(4). Therefore, Eq.(1.5) is still correct. From this example, we may get an illusion that the inclusion of the source term on the flux evaluation is not necessary. However, if we look careful at the initial data of Fig.(4), the h distribution itself around a cell interface has different slopes, see Fig.(5). The fortunate point in SGM is that only the pointwise flow variables at the cell interface is used in the flux evaluation (like most other Riemann solvers). For a high accurate scheme under the initial condition of Fig.(5), if the different slopes of h are used to construct a time-dependent flux function, such as the case in the Generalized Riemann solver, without considering the source term from different bottom shapes the gas evolution of the homogeneous equations will give a flux function different from a purely pressure contribution in Eq.(1.5). So, in order to keep Eq.(1.5) true even when we solve the initial value problem with the inclusion of different h slopes in Fig.(5), we have to include the source term effect in the flux evaluation as well. For a well balanced scheme, the source term contribution has to precisely match the effect from different h slopes in this case in order to have a final flux function, which has a time-independent pressure contribution only at a cell interface.

In terms of gas kinetic schemes for the shallow water equations, a fractional step method is obtained in [6]. Since the source term is not included in the flux evaluation, the BGK scheme presented in [6] is not a well balanced scheme, and it cannot keep the equilibrium state $U = 0$ and $h + B =$ constant exactly. Slyz and Prendergast [13] has extended the gas-kinetic BGK scheme to the Euler equations with gravitational force. They also used a fractional step method, where the flux evaluation is based on the homogeneous Euler equations. As analyzed in [13], the reason for them to ignore the source term on the flux evaluation is that the gravitational force has only higher order effect on the particle trajectory, such that $x = x' + u'(t - t') + \Phi_x(t - t')^2$, where the gravitational term is proportional to $(t - t')^2$. For a scheme with 2nd order accuracy in time, i.e. the gas evolution being proportional to t, the higher order term can be ignored. However, as pointed out in the current paper, the above analysis is incomplete. It is true that the gravitational force Φ_x has a high order effect on the particle trajectory, but it has a first order effect on the particle velocity $u = u' + \Phi_x(t - t')$. Due to the gravitational force, the change of particle velocity has a direct influence on the variation of the gas distribution function. Its contribution to the fluid motion is on the same order as those from the linear spatial variation of the flow variables, such as the water height or velocity gradients. Recently, Audusse et. al. has developed a 1st-order kinetic flux vector splitting scheme based on the collisionless Boltzmann equation for the shallow water equations with source term [2]. With the appropriate choice of the flux splitting, their scheme is a well balanced one in the case of $U = 0$ and $h + B =$ constant. But, the applicability of the scheme to the tough problems, such as LeVeque's sound wave propagation test, needs further verification.

In order to develop an accurate and physically reliable scheme, which follows the real fluid motion as close as possible, the source term needs to be taken into account explicitly in the flux evaluation. The current paper presents such a scheme, where the time-dependent flux is obtained by solving the gas-kinetic BGK model for the linearly distributed initial flow variables and bed profile around a cell interface, see Fig.(6). In the special case of Fig.(5), the current scheme could keep the exact solution of $U = 0$ and $h + B =$ constant.

2 A BGK Scheme for the Shallow Water Equations

We consider the shallow water equations with source term:

$$\begin{pmatrix} h \\ hU \end{pmatrix}_t + \begin{pmatrix} hU \\ hU^2 + \frac{1}{2}Gh^2 \end{pmatrix}_x = \begin{pmatrix} 0 \\ -B'(x)Gh \end{pmatrix}. \tag{2.6}$$

In this system, h is the water height, U the velocity, and G the gravitational constant. $B(x)$ is the topology of the river bottom. The numerical discretization of the above equation with $W = (h, hU)^T$ is

$$W_j^{n+1} - W_j^n = \frac{1}{\Delta x}\int_{t^n}^{t^{n+1}} \left(F_{j-1/2}(t) - F_{j+1/2}(t)\right) dt + \frac{1}{\Delta x}\int_{x_{j-1/2}}^{x_{j+1/2}}\int_{t^n}^{t^{n+1}} S(W) dx dt,$$

and in this paper the source term is always discretized as

$$\frac{1}{\Delta x}\int_{x_{j-1/2}}^{x_{j+1/2}}\int_{t^n}^{t^{n+1}} S(W) dx dt = -\Delta t \frac{(h_j^n + h_j^{n+1})}{2} B'(x_j) G,$$

where $B'(x_j)$ is the bed slope at the center of cell j. The scheme presented in this section is mainly about the construction of a time-dependent numerical fluxes $F_{j+1/2}(t)$ under the general initial condition of Fig.(6) by solving the gas-kinetic BGK model [4].

The generalized BGK model with the inclusion of the gravitational force can be written as

$$f_t + u f_x + \Phi_x f_u = \frac{g - f}{\tau}, \tag{2.7}$$

where f is the gas distribution function and g the equilibrium state f approaches. τ is the particle collision time and Φ_x is the gravitational acceleration due to the wary river bottom $\Phi_x = -GB'(x)$.

For the shallow water equations, f and g are functions of space x, time t, and particle velocity u. The equilibrium state g which maximizes the entropy for the shallow water system is a Maxwellian distribution [6],

$$g = h\left(\frac{\lambda}{\pi}\right)^{\frac{1}{2}} e^{-\lambda(u-U)^2},$$

where λ is defined by $\lambda = 1/(hG)$. Due to the conservation property in particle collisions, f and g satisfy the compatibility condition

$$\int (f - g)\psi_\alpha du = 0 \qquad \text{for} \qquad \psi_\alpha = (1, u)^T, \tag{2.8}$$

at any point in space and time.

The integral solution of the BGK model is

$$f(x_{j+1/2}, t, u) = \frac{1}{\tau}\int_0^t g(x', t', u') e^{-(t-t')/\tau} dt' + e^{-t/\tau} f_0(x_0, u_0), \tag{2.9}$$

where $x_{j+1/2}$ is the location of the cell interface and $x_{j+1/2} = x' + u'(t-t') + \frac{1}{2}\Phi_x(t-t')^2$ is the particle trajectory. Also, due to the gravitational force, the particle velocity will change according to Newton's law $u = u' + \Phi_x(t - t')$. Therefore, x_0 and u_0 in the initial term f_0 become $x_0 = x_{j+1/2} - u_0 t - \frac{1}{2}\Phi_x t^2$

and $u_0 = u - \Phi_x t$. There are two unknowns in the above equation. One is the initial gas distribution function f_0 at time $t = 0$, and the other is the equilibrium state g in both space and time locally around $(x_{j+1/2}, t = 0)$.

Before we go to construct the gas-kinetic scheme based on the above integral equation, let's first consider the particle velocity change due to the gravitational force and its modification to the gas distribution function. In the derivation below, terms on the order of t^2 will be ignored automatically. Suppose that a particle is moving from x' to x in a short time interval $t-t'$. Because of the gravitational acceleration, the particle velocity will change from u' to u and the relation is $u = u' + \Phi_x(t - t')$. So, due to the particle velocity change, an equilibrium state g_0 at time t' can be expressed as,

$$\begin{aligned} g_0 &= h(\frac{\lambda}{\pi})^{\frac{1}{2}} e^{-\lambda(u'-U)^2} \\ &= h(\frac{\lambda}{\pi})^{\frac{1}{2}} e^{-\lambda[(u-\Phi_x(t-t'))-U]^2} \\ &= h(\frac{\lambda}{\pi})^{\frac{1}{2}} e^{-\lambda(u-U)^2} e^{2\lambda\Phi_x(u-U)(t-t')-\lambda\Phi_x^2(t-t')^2} \\ &= g e^{2\lambda\Phi_x(u-U)(t-t')-\lambda\Phi_x^2(t-t')^2}, \end{aligned}$$

where g is the equilibrium state at time t. Note that in the above equation, only particle velocity change is accounted. Using the Taylor expansion and neglecting the higher order terms, the above equilibrium state can be approximated as

$$g_0 \simeq g\left[1 + 2\lambda\Phi_x(u - U)(t - t')\right].$$

The term $2\lambda\Phi_x(u-U)(t-t')g$ in the above equation presents the variation of the distribution function due to particle velocity change. Due to the Taylor expansion, the above equilibrium state g_0 deviates from an exact Maxwellian distribution. In order to compensate for the non-Maxwellian and the ignored all high order terms, we are going to put one more constant α in Φ_x term and express g_0 as

$$g_0 = g\left[1 + 2\alpha\lambda\Phi_x(u - U)(t - t')\right].$$

The value of α depends on the moments $(1, u, u^2)^T$ taken by the above distribution function. As analyzed later for a well balanced scheme, α will have the following constant values when taking different moments,

$$\alpha_1 = 3/4, \alpha_u = 1, \alpha_{u^2} = 5/4.$$

The time evolution of the distribution function in space and time due to other factors, such as the velocity and water depth gradients, will be given later. The gravitational force Φ_x for the condition in Fig.(6) can be written as

$$\Phi_x = -G\left(B'_j(1 - H[x]) + B'_{j+1}H[x]\right), \tag{2.10}$$

where $H[x]$ is the Heaviside function, and B'_j and B'_{j+1} are the constant slopes in cell j and $j + 1$. The following is the numerical procedures to get the solution of Eq.(2.9).

Step(1): With the cell averaged data h_j and h_jU_j, we are going to use Surface Gradient Method (SGM) to get the initial data interpolation for the water height h and momentum hU [18]. In the SGM, the nonlinear limiter is used on the water surface height $\eta_j = h_j + B_j$ and the momentum h_jU_j. After the MUSCL-type interpolation, the flow distributions $W_j = (h_j, h_jU_j)^T$ around a cell interface $x_{j+1/2}$ can be described as

$$W_j(x) = W_j(x_j) + \frac{W_j(x_{j+1/2}) - W_j(x_{j-1/2})}{x_{j+1/2} - x_{j-1/2}}(x - x_j) \quad \text{for} \quad x \in [x_{j-1/2}, x_{j+1/2}], \tag{2.11}$$

where the water heights at the left and right hand side of a cell interface $x_{j+1/2}$ are

$$h_j(x_{j+1/2}) = \eta_j(x_{j+1/2}) - B(x_{j+1/2}) \quad \text{and} \quad h_{j+1}(x_{j+1/2}) = \eta_{j+1}(x_{j+1/2}) - B(x_{j+1/2}).$$

There is a possible discontinuity between $W_j(x_{j+1/2})$ and $W_{j+1}(x_{j+1/2})$, see Fig.(6).

Step(2): Based on the reconstructed data in Step(1), around each cell interface $x_{j+1/2}$, we can construct an initial gas distribution function f_0 [1],

$$\begin{aligned} f_0(x,u) &= g^l\left(1 + a^l(x - x_{j+1/2})\right)\left(1 - H[x - x_{j+1/2}]\right) \\ &\quad + g^r\left(1 + a^r(x - x_{j+1/2})\right)H[x - x_{j+1/2}], \end{aligned} \tag{2.12}$$

where the states g^l and g^r are the Maxwellian distribution functions which have the one-to-one correspondence with the conservative variables at cell interface,

$$g^l = g^l(W_j(x_{j+1/2})) \qquad \text{and} \qquad g^r = g^r(W_{j+1}(x_{j+1/2})).$$

For example, with the distribution

$$g^l = h^l\left(\frac{\lambda^l}{\pi}\right)^{\frac{1}{2}} e^{-\lambda^l(u-U^l)^2},$$

all coefficients in g^l can be obtained as

$$\begin{pmatrix} h^l \\ U^l \\ \lambda^l \end{pmatrix} = \begin{pmatrix} h_j(x_{j+1/2}) \\ h_jU_j(x_{j+1/2})/h_j(x_{j+1/2}) \\ 1/(Gh^l) \end{pmatrix}.$$

Similar equations can be found for g^r. The parameters $a^{l,r}$ in Eq.(2.12) are from the Taylor expansion of a Maxwellian and have the form

$$a^{l,r} = m_1^{l,r} + m_2^{l,r}u + m_3^{l,r}u^2.$$

[1] Since we are not solving viscous shallow water equations, the non-equilibrium part in f_0, which contributes mostly to low Reynolds number flow, is ignored in the initial gas distribution function. For a viscous flow simulation, the Chapman-Enskog expansion needs to be used, see [17] for detail. The simulations results presented in section 3 are almost identical for the scheme with or without the non-equilibrium term in f_0.

The coefficients $(m_1^{l,r}, m_2^{l,r}, m_3^{l,r})$ are determined from $(h^l, h^l U^l)$ and $(h^r, h^r U^r)$ and their initial slopes in cell j and $j+1$,

$$\left(\frac{\partial h^l}{\partial x}, \frac{\partial (hU)^l}{\partial x}\right) \qquad \text{and} \qquad \left(\frac{\partial h^r}{\partial x}, \frac{\partial (hU)^r}{\partial x}\right).$$

The relations are

$$\begin{aligned} m_1^{l,r} &= \left[(\frac{1}{2h} + \frac{3U^2}{Gh^2}) \frac{\partial h}{\partial x} - \frac{2U}{Gh^2} \frac{\partial (hU)}{\partial x} \right]^{l,r}, \\ m_2^{l,r} &= \left[-\frac{4U}{Gh^2} \frac{\partial h}{\partial x} + \frac{2}{Gh^2} \frac{\partial (hU)}{\partial x} \right]^{l,r}, \\ m_3^{l,r} &= \left[\frac{1}{Gh^2} \frac{\partial h}{\partial x} \right]^{l,r}. \end{aligned} \tag{2.13}$$

So, all coefficients in Eq.(2.12) can be determined from the initially reconstructed data in Step(1). For simplification, we will assume $x_{j+1/2} = 0$ in the rest of this paper.

Eq.(2.12) shows the gas distribution function f at time $t = 0$. When taking f_0 into the integral solution (2.9), we will calculate the particle with velocity u arriving $x = 0$ at time t,

$$\begin{aligned} f_0(-ut - \frac{1}{2}\Phi_x t^2, u - \Phi_x t) &= g_0^l \left(1 + a^l(-ut - \frac{1}{2}\Phi_x t^2)\right) \left(1 - H(-ut - \frac{1}{2}\Phi_x t^2)\right) \\ &\quad + g_0^r \left(1 + a^r(-ut - \frac{1}{2}\Phi_x t^2)\right) H(-ut - \frac{1}{2}\Phi_x t^2) \\ &\simeq g_0^l \left(1 - uta^l\right) H(u) + g_0^r \left(1 - uta^r\right)(1 - H(u)), \end{aligned}$$

where all terms proportional to t^2 has been ignored. The states g_0^l and g_0^r are different from the states g^l and g^r in Eq.(2.12) due to the particle velocity change from time $t = 0$ to t. The relations between g_0^l, g_0^r, g^l and g^r are

$$g_0^l = g^l \left(1 + 2\alpha\lambda^l \Phi_x (u - U^l) t\right)$$

and

$$g_0^r = g^r \left(1 + 2\alpha\lambda^r \Phi_x (u - U^r) t\right).$$

Therefore,

$$\begin{aligned} f_0(-ut - \frac{1}{2}\Phi_x t^2, u - \Phi_x t) &\simeq g^l \left(1 + 2\alpha\lambda^l \Phi_x (u - U^l) t\right) \left(1 - uta^l\right) H(u) \\ &\quad + g^r \left(1 + 2\alpha\lambda^r \Phi_x (u - U^r) t\right) \left(1 - uta^r\right)(1 - H(u)). \end{aligned}$$

We can further simplify the above expression to

$$\begin{aligned} f_0(-ut - \frac{1}{2}\Phi_x t^2, u - \Phi_x t) &\simeq g^l \left(1 + 2\alpha\lambda^l \Phi_x (u - U) t - uta^l\right) H(u) \\ &\quad + g^r \left(1 + 2\alpha\lambda^r \Phi_x (u - U) t - uta^r\right)(1 - H(u)). \end{aligned} \tag{2.14}$$

From the above equation, we can see that the gravitational force contributes to particle distribution function change on the same order as the terms a^l and a^r. The claim in [13] is inappropriate. Due to the characteristic line $x = x' + u'(t - t') + \frac{1}{2}\Phi_x (t - t')^2$ in the particle movement, the Heaviside function in Φ_x of Eq.(2.10) becomes approximately $H[x'] = H[-u(t-t')]$. Since $t > t'$, the gravitational force term in Eq.(2.14) has the form

$$\Phi_x = -G\left(B'_j H[u] + B'_{j+1}(1 - H[u])\right).$$

The physical meaning of the above equation is that in terms of the moving particles toward the cell interface (forming fluxes), the left bottom slope B'_j will effect these particles with velocity $u > 0$ and the right slope B'_{j+1} to the particle with velocity $u < 0$. Since we truncate the expansion to the order proportional to t, those particles which could turn around (U-turn) in a short time $t - t'$ has be neglected in the above approximation.

Step(3): After constructing the initial state f_0, the equilibrium state g is assumed to be continuous across a cell interface but with different slopes at the left and right hand sides,

$$g = g_0\left(1 + (1 - \mathrm{H}[x])\bar{a}^l x + \mathrm{H}[x]\bar{a}^r x + \bar{A}t\right), \tag{2.15}$$

where g_0 is the equilibrium state located at $x = 0$ and $t = 0$,

$$g_0 = h_0(\frac{\lambda_0}{\pi})^{\frac{1}{2}} e^{-\lambda_0(u-U_0)^2}.$$

Here $\bar{a}^l, \bar{a}^r$, and $\bar{A}$ in Eq.(2.15) have the forms

$$\bar{a}^{l,r} = \bar{m}_1^{l,r} + \bar{m}_2^{l,r} u + \bar{m}_3^{l,r} u^2,$$

$$\bar{A} = \bar{A}_1 + \bar{A}_2 u + \bar{A}_3 u^2. \tag{2.16}$$

Taking both limits ($x \to 0, t \to 0$) in Eq.(2.9) and (2.15), and applying the compatibility condition (2.8) at ($x = 0, t = 0$), the macroscopic variables corresponding to g_0 can be uniquely determined in terms of f_0,

$$W_0 = \begin{pmatrix} h_0 \\ h_0 U_0 \end{pmatrix} = \int g_0 \psi_\alpha du = \int [g^l \mathrm{H}(u) + g^r(1 - \mathrm{H}(u))]\psi_\alpha du, \tag{2.17}$$

where W_0 is the "averaged " flow variables at the cell interface. Then, connecting W_0 to the cell centered values $W_j(x_j)$ and $W_{j+1}(x_{j+1})$, we can get two slopes for mass and momentum separately

$$\left(\frac{\partial h_0^l}{\partial x}, \frac{\partial (hU)_0^l}{\partial x}\right)^T = \frac{W_0 - W_j(x_j)}{x_{j+1/2} - x_j} \qquad \text{for} \qquad x \leq 0,$$

$$\left(\frac{\partial h_0^r}{\partial x}, \frac{\partial (hU)_0^r}{\partial x}\right)^T = \frac{W_{j+1}(x_{j+1}) - W_0}{x_{j+1} - x_{j+1/2}} \qquad \text{for} \qquad x \geq 0, \tag{2.18}$$

from which $(\bar{a}^l, \bar{a}^r)$ can be determined in a similar way as shown in Eq.(2.13). Now, the unknown in Eq.(2.15) is $\bar{A}$, which can be expressed as

$$\bar{A}_1 = \left(\frac{1}{2h_0} + \frac{3U_0^2}{Gh_0^2}\right)\frac{\partial h_0}{\partial t} - \frac{2U_0}{Gh_0^2}\frac{\partial (hU)_0}{\partial t},$$

$$\bar{A}_2 = -\frac{4U_0}{Gh_0^2}\frac{\partial h_0}{\partial t} + \frac{2}{Gh_0^2}\frac{\partial (hU)_0}{\partial t},$$

$$\bar{A}_3 = \frac{1}{Gh_0^2}\frac{\partial h_0}{\partial t}, \tag{2.19}$$

where $\partial h_0/\partial t$ and $\partial(hU)_0/\partial t$ need to be determined. In the above equilibrium state, we do not include the gravitational force to the particle velocity change. This effect will be included in the integral solution (2.9) in the following way. For an equilibrium state $g(x',t',u')$ at x' and t', its particle will get to $x = 0$ at time $t - t'$. During this particle transport process, the particle velocity u' will be changed to u through the relation $u = u' + \Phi_x(t - t')$. With the consideration of the gravitational force effect during the time interval $(t - t')$, the integration of $g(x', t', u')$ in Eq.(2.9) becomes

$$\begin{aligned}\int_0^t g(x',t',u')e^{-(t-t')/\tau}dt' &= \int_0^t g_0 \Big[1 - u(t-t')\left(\bar{a}^l H[u] + \bar{a}^r(1 - H[u])\right) \\ &\quad + \bar{A}t' + 2\alpha\lambda_0\Phi_x(u - U_0)(t-t')\Big]\, e^{-(t-t')/\tau}dt',\end{aligned} \tag{2.20}$$

where the particle velocity change has been included. Due to the integration on the characteristic line $x = x' + u'(t - t')$, Φ_x has the form

$$\Phi_x = -G\left({B'}_j H[u] + {B'}_{j+1}(1 - H[u])\right).$$

Step(4): Substitute Eq.(2.14) and (2.20) into the integral solution (2.9), we can obtain the distribution function f at $x = 0$,

$$\begin{aligned} f(0,t,u) &= \gamma_0 g_0 \\ &\quad + \gamma_1 \left[\left(\bar{a}^l \mathrm{H}[u] + \bar{a}^r(1 - \mathrm{H}[u])\right)u + 2\alpha\lambda_0\Phi_x(u - U_0)\right] g_0 \\ &\quad + \gamma_2 \bar{A} g_0 \\ &\quad + \gamma_3\left(\mathrm{H}[u]g^l + (1 - \mathrm{H}[u])g^r\right) \\ &\quad + \gamma_3\Big[-t\left(ua^l + 2\alpha\lambda^l\Phi_x(u - U^l)\right)\mathrm{H}[u]g^l \\ &\quad - t\left(ua^r + 2\alpha\lambda^r\Phi_x(u - U^r)\right)(1 - \mathrm{H}[u])g^r\Big]\end{aligned} \tag{2.21}$$

where

$$\gamma_0 = 1 - e^{-t/\tau},$$

$$\gamma_1 = \tau(-1 + e^{-t/\tau}) + te^{-t/\tau},$$

$$\gamma_2 = \tau(t/\tau - 1 + e^{-t/\tau}),$$

$$\gamma_3 = e^{-t/\tau}.$$

As pointed out earlier, there are two unknowns $(\partial h_0/\partial t, \partial(hU)_0/\partial t)$ in $\bar{A}$ of Eq.(2.21). Since the compatibility condition must be satisfied everywhere in space and time, it can be integrated in a whole CFL time step Δt at $x = 0$

$$\int_0^{\Delta t}\int \left(f(0,t,u) - g(0,t,u)\right)\psi_\alpha dt du = 0, \tag{2.22}$$

from which we have

$$
\begin{aligned}
\left(\frac{\partial h_0}{\partial t}, \frac{\partial (hU)_0}{\partial t}\right)^T &= \int \Big[\Gamma_1 \left(\bar{a}^l \mathrm{H}[u] + \bar{a}^r (1-\mathrm{H}[u])\right) u g_0 \\
&+ \Gamma_1 \left({B'}_j \mathrm{H}[u] + {B'}_{j+1}(1-\mathrm{H}[u])\right) 2\alpha\lambda_0 G(u-U_0) g_0 \\
&+ \Gamma_2 \left(a^l u \mathrm{H}[u] g^l + a^r u (1-\mathrm{H}[u]) g^r\right) \\
&+ \Gamma_2 \left(2\alpha\lambda^l (u-U^l) {B'}_j \mathrm{H}[u] g^l + 2\alpha\lambda^r (u-U^r) {B'}_{j+1} \mathrm{H}[u] g^r\right)\Big] \psi_\alpha du. \qquad (2.23)
\end{aligned}
$$

All terms on the right hand side of the above equation are known and

$$
\begin{aligned}
\Gamma_0 &= \Delta t - \tau(1-e^{-\Delta t/\tau}), \\
\Gamma_1 &= \left(-\Delta t + 2\tau(1-e^{-\Delta t/\tau}) - \Delta t e^{-\Delta t/\tau}\right)/\Gamma_0, \\
\Gamma_2 &= \left(\Delta t e^{-\Delta t/\tau} - \tau(1-e^{-\Delta t/\tau})\right)/\Gamma_0.
\end{aligned}
$$

So, $\bar{A}$ in Eq.(2.16) is totally determined.

Step(5): The time-dependent numerical fluxes of mass and momentum across the cell interface can be obtained by integrating Eq.(2.21),

$$
\begin{pmatrix} F_h(t) \\ F_{hU}(t) \end{pmatrix}_{j+1/2} = \int u \begin{pmatrix} 1 \\ u \end{pmatrix} f_{j+1/2}(0,t,u) du. \qquad (2.24)
$$

Even with different slopes of h and B on both sides of a cell interface, it is not difficult to prove that the above kinetic scheme could keep an exact equilibrium solution with $U=0$ and $h_j + B_j =$ constant, see Fig.(4). In this equilibrium case, in order to make the above flux function in Eq.(2.24) have the constant pressure contribution only, such as $(F_h(t)=0, F_{hU}(t) = Gh^2_{j+1/2}(0)/2)$ at a cell interface, the coefficient α associated with the integration of the gravitational term have to take the values $\alpha_1 = 3/4, \alpha_u = 1, \alpha_{u^2} = 5/4$ when taking different moments. Equipped with these constant coefficients, the gas kinetic BGK scheme is a well balanced method. Numerically, for the fluid with the equilibrium initial data, the BGK scheme will keep such a solution to the order of machine accuracy. For unsteady, transcritical and all other flow computations, the same constant coefficients are used.

For most engineering applications, if the efficiency is the main concern, the above BGK scheme can be much simplified by removing particle collisional term. The gas distribution function based on the collisionless Boltzmann equation becomes

$$
\begin{aligned}
f(0,t,u) &= \left(\mathrm{H}[u] g^l + (1-\mathrm{H}[u]) g^r\right) \\
&+ \Big[-t\left(ua^l + 2\alpha\lambda^l \Phi_x (u-U^l)\right) \mathrm{H}[u] g^l \\
&\quad -t\left(ua^r + 2\alpha\lambda^r \Phi_x (u-U^r)\right)(1-\mathrm{H}[u]) g^r\Big],
\end{aligned}
$$

and the numerical flux can be evaluated similarly as Eq.(2.24) by using the above f. This scheme is called the kinetic flux vector splitting (KFVS) method, which has close relation to flux vector splitting scheme. The above simplified scheme is also a well balanced method to keep the steady state $U=0$ and $h+B=$ constant exactly. It works for all test cases shown in the next section except more diffusive in the simulation results. The dissipation in the above simplified scheme is on the same order as other flux vector splitting (FVS) schemes or the HLL method. Since we are not solving the viscous shallow water equations, additional dissipation will not be so harmful. We believe that due to the consideration of the whole spectrum of particle velocities in the above KFVS scheme it will be more robust than any other schemes based on the Riemann solution we can construct for the shallow water equations with source terms. Since we incorporate all slopes of h, hU, and B in the above gas evolution distribution function, it is different from the kinetic approach in [2], even they are based on solving the same collisionless Boltzmann equation.

3 Numerical Examples

In this section, we are going to test the gas-kinetic scheme in 1D case, which cover many tough ones, such as LeVeque's sound wave propagation cases and transcritical ones. In all calculations, the collision time τ takes the values

$$\tau = \mathcal{C}_1 \Delta t + \mathcal{C}_2 \Delta t \frac{|h^l h^l - h^r h^r|}{h^l h^l + h^r h^r}, \tag{3.25}$$

where $C_1 = 0.05, C_2 = 1.0$. As analyzed previously for the compressible Euler and Navier-Stokes equations, usually the first term on the right hand side of τ should be related to physical viscosity coefficient and the second one is used to provide the artificial dissipation once needed in the under-resolved region. Since all test cases in this section are targeted to the inviscid shallow water equations, the physical viscous term is replaced by a numerical value. Due to the inclusion of the particle collisional effect in the BGK model, the current scheme has less dissipation than the KFVS scheme. In the calculations, the time step Δt is determined from the CFL condition and different CFL numbers, such as $0.1, 0.5$ and 0.8, have been tested. The simulation results are basically not sensitive to these change. As pointed out earlier, all initial interpolation is based on the van Leer limiter. Except specifically pointing out, the gravitational constant G takes the value 9.8.

Case (1):

Here we test two standard shock tube problems, where the homogeneous shallow water equations are solved. The initial condition for the first example is

$$(h_l = 1.0, U_l = 0.0)|_{x<0.5} \qquad \text{and} \qquad (h_r = 0.1, U_r = 0.0)|_{x\geq 0.5}.$$

The simulation results h and hU with 100 grid points at the output time $t = 0.3$ are shown in Fig.(7) and (8), where the solid lines are the exact solutions. From this test case, we can understand that the gas-kinetic BGK scheme has a good shock capturing ability. In the second example, we consider the shallow water solution with two strong rarefaction waves. The initial condition is

$$(h_l = 1.0, U_l = -5.0)|_{x<0.5} \qquad \text{and} \qquad (h_r = 0.1, U_r = 5.0)|_{x\geq 0.5}.$$

The simulation results h and U with 100 grid points at the output time $t = 2.5$ are shown in Fig.(9) and (10), where the solid lines are the exact solutions. As pointed out by Toro [14], most upwinding schemes could get failed in this test. Even with very inaccurate solution, the Godunov method with exact Riemann solution needs dry bed condition to pass this test. But, the exact solution for this problem has not gotten to the dry condition (vacuum) yet. The BGK scheme can pass this test without any difficulty.

Case (2):

This is a steady state case to check both the dissipative and phase errors in the kinetic scheme. The bottom shape of the river has the form

$$B(x) = 0.2e^{-(x+1)^2/2} + 0.3e^{-(x-1.5)^2}.$$

The computational domain is on the range $x \in (-10, 10)$, and the left boundary condition is $U_- = 1.0, h_- = 1.0$. The equilibrium state can be obtained exactly for this problem, see Fig.(11). The numerical solutions U and $h + B$ obtained with 100 and 50 grid points are shown in Fig.(12). Even with the coarse mesh, such as $\Delta x = 0.4$, accurate solutions can be obtained.

Case (3):

This is an unsteady test problem proposed by Bermudez and Vazquez [3]. The bed topography is defined by

$$B(x) = 10 + \frac{40x}{L} + 10\sin\left[\pi(\frac{4x}{L} - \frac{1}{2})\right],$$

where $L = 14,000m$ is the channel length. The initial and boundary conditions are

$$h(x,0) = 60.5 - B(x) \quad , \quad U(x,0) = 0,$$

and

$$h(0,t) = 64.5 - 4.0\sin\left[\pi(\frac{4t}{86,400} + \frac{1}{2})\right] \quad , \quad U(L,t) = 0.0.$$

With the above conditions, there is an approximate solution based on the asymptotic analysis given in [3],

$$h(x,t) = 64.5 - B(x) - 4\sin\left[\pi(\frac{4t}{86,400} + \frac{1}{2})\right],$$

and

$$U(x,t) = \frac{(x-L)\pi}{5400h(x,t)}\cos\left[\pi(\frac{4t}{86,400} + \frac{1}{2})\right].$$

The simulations results from the BGK scheme at output time $t = 7552.13s$ with $\Delta x = 280m$ (50 cells in L) are presented in Fig.(13) and (14), where the solid lines are exact solutions. The agreement between the numerical and exact solutions are excellent.

Case (4):

These are classical test problems for transcritical and subcritical flows. They are widely used to test numerical scheme for the shallow water equations. The 1D simulation channel has a length of $25m$. The bed profile is given by

$$B(x) = \begin{cases} 0.2 - 0.05(x-10)^2, & \text{for } 8 < x < 12, \\ 0.0, & \text{otherwise.} \end{cases}$$

Depending on the initial and boundary conditions, the flow may be subcritical, transcritical with or without a steady shock, or supercritical. Since the transcritical cases are more difficult, we only include these two cases here. In both cases, the physical domain is covered with 200 cells with the cell size $\Delta x = 0.125m$.

For the transcritical case without a shock, a discharge per unit width of $hU = 1.53m^2/s$ was imposed as the upstream boundary condition. The steady state solutions for both hU and $h + B$ are shown in Fig.(15) and (16). As noticed by many authors, the correct capturing of the discharge hU is usually more difficult than the water height $h+B$. For the transcritical flow with a shock, the discharge has a value $hU = 0.18m^2/s$ at the upstream boundary and $h = 0.33m$ is imposed as the downstream boundary condition. The simulations results of hU, $h + B$ and Froude number $Fr = U/\sqrt{Gh}$ are shown in Fig.(17), (18) and (19). Like the scheme in [18], there exists overshoot in the Fr distribution. Comparing the above results with those obtained from the KFVS-type kinetic method [2], we can see clearly that the current method has a higher accuracy, such as in the solution of flow discharge.

Case (5):

This case is about sound wave propagation proposed by LeVeque in [11]. The channel has a length 1.0 and the channel bottom has the topography defined by

$$B(x) = \begin{cases} 0.25(\cos(\pi(x-0.5)/0.1) + 1.0), & \text{for } |x-0.5| \leq 0.1, \\ 0.0, & \text{otherwise.} \end{cases}$$

The data are initially stationary ($U = 0$) with a surface profile defined by

$$h(x) = \begin{cases} 1.0 - B(x) + \epsilon, & \text{for } 0.1 < x < 0.2, \\ 1.0 - B(x), & \text{otherwise.} \end{cases}$$

Two cases have been run with $\epsilon = 0.2$ and 0.01. The solutions with 100 and 200 grid points and $G = 1.0$ shown in Fig.(20)-(23). The case with $\epsilon = 0.01$ is a very tough one. Most previous calculations for this case used much more grid points, such as 600 in [9]. We believe that the simulation with 100 or 50 grid points can fail many currently existing well balanced schemes. From this case, we can understand that the gas-kinetic scheme can capture the quasi-steady solutions as good as LeVeque's scheme. But, the kinetic scheme can also capture the transcritical flow with shocks without any difficulty.

We do not include any 2D test in this section. Actually, even for the fractional step BGK scheme [6], it does a very good job in 2D simulations. The current scheme is at least as robust as the fractional step method, but it is more accurate.

4 Conclusion

In this paper, we have developed a gas-kinetic BGK scheme for the shallow water equations with source term. Due to the gravitational acceleration to the fluid particle, the source term effect is explicitly included in the time-evolution of the gas distribution function at a cell interface, from which the numerical flux is obtained. The current method is a well balanced scheme and very robust for both steady and unsteady flow simulations. This is not surprising because the kinetic scheme is intrinsically solving the viscous governing equations. Perfect simulation results are obtained for many tough problems. The success of the kinetic method is coming from its underlying design principle:

the numerical fluid evolution should follow the flow physics as close as possible. The physical reality for the shallow water equations with source term is that the gravitational force is existing everywhere, it will not only effect the fluid motion inside each numerical cell (second term on the right hand side of Eq.(1.2)), but also act on these fluid passing through the cell interface (first term on the right hand side of Eq.(1.2)). Even with standard central discretization for the second term on the right hand side of Eq.(1.2), a well balanced scheme can still be obtained when the gravitational effect is correctly included in fluid motion across a cell interface. The importance of including source term in the flux evaluation has been emphasized earlier for the Euler equations with heat transfer [16]. Even for the compressible Euler and Navier-Stokes equations, the success of the gas-kinetic BGK scheme in comparison with other flux vector splitting schemes are also due to the including of source term (particle collisions in the Boltzmann equation) in the gas evolution process. At end, we should realize that there is no a general numerical scheme for the hyperbolic system with source terms. The dynamical influence on the fluid motion from different source term has to be modeled and implemented case by case.

Acknowledgments

The current research is supported by the Research Grant Council of Hong Kong through HKUST6132/00P.

References

[1] F. Alcrudo and F. Benkhaldoun, Exact solutions to the Riemann problem of the shallow water equations with a bottom step, *Computers & Fluids* **30**, pp. 643-671 (2001).

[2] E. Audusse, M.O. Bristeau, and B. Perthame, Kinetic schemes for Saint-Venant equations with source terms on unstructured grids, *INRIA report No. 3989* (2000).

[3] A. Bermudez, M.E. Vazquez, Upwind methods for hyperbolic conservation laws with source terms, *Computers Fluids* **23**, No.8, 1049-1071 (1994).

[4] P.L. Bhatnagar, E.P. Gross, and M. Krook, A model for collision processes in gases I: small amplitude processes in charged and neutral one-component systems, *Phys. Rev.* **94**, pp. 511-525 (1954).

[5] V.T. Chow, Open-channel hydraulics, *McGraw-Hill Book Company, New York* (1959).

[6] M.S. Ghidaoui, J.Q. Deng, W.G. Gray, and K. Xu, A Boltzmann based model for open channel flows, *Int. J. Numer. Meth. Fluids* **35**, 449-494 (2001).

[7] P. Glaister, Approximate Riemann solutions of the shallow water equations, *J. Hydraulic Research* **26**, No.3, 293-306 (1988).

[8] J.M. Greenberg, A. Y. Lerroux, A well-balanced schemes for the numerical processing of source terms in hyperbolic equations, *SIAM J. Numer. Anal.* **33**, No.1, 1-16 (1996).

[9] M.E. Hubbard and P. Garcia-Navarro, Flux difference splitting and the balancing of source terms and flux gradients, *J. Comput. Phys.*, **165**, pp. 89-125 (2000).

[10] P. Jenny and B. Muller, Rankine-Hugoniot-Riemann solver considering source terms and multidimensional effects, *J. Comput. Phys.*, **145**, pp. 575-610 (1998).

[11] R.J. LeVeque, Balancing source terms and flux gradients in high-resolution Godunov methods: the quasi-steady wave-propagation algorithm. *J. Comput. Phys.*, **146**, pp. 346 (1998).

[12] A. Noussair, Riemann problem with nonlinear resonance effects and well-balanced Godunov scheme for Shallow water fluid flow past an obstacle, *SIAM J. Numer. Anal.*, **39**, No.1, pp. 52-72 (2001).

[13] A. Slyz and K.H. Prendergast, Time-independent gravitational fields in the BGK scheme for hydrodynamics, *Astron. Astrophys. Suppl. Ser.* **139**, pp. 199-217 (1999).

[14] E.F. Toro, Shock-capturing methods for free-surface shallow flows, *John Wiley & Sons, Ltd.*, England (2001).

[15] M.E. Vazquez-Cendon, Improved treatment of source terms in upwind schemes for the shallow water equations in channels with irregular geometry, *J. Comput. Phys.* **148**, pp. 497-526 (1999).

[16] K. Xu, A gas-kinetic scheme for the Euler equations with heat transfer, *SIAM J. Sci. Comput.* **20**, pp. 1317-1335 (1999).

[17] K. Xu, A gas-kinetic BGK scheme for the Navier-Stokes equations and its connection with artificial dissipation and Godunov method, to appear in *J. Comput. Phys.* (2001).

[18] J.G. Zhou, D.M. Causon, C.G. Mingham, and D.M. Ingram, The surface gradient method for the treatment of source terms in the shallow water equations, *J. Comput. Phys.*, **168**, 1-25 (2001).

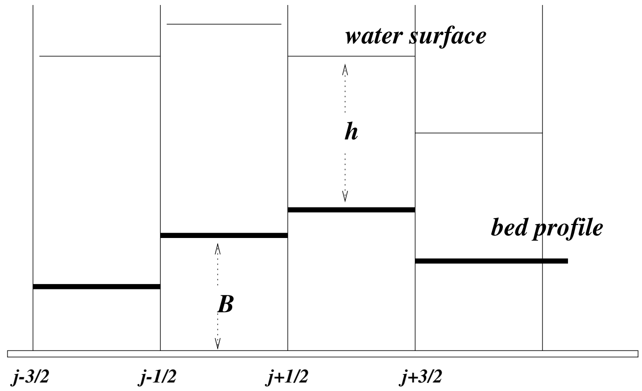

Figure 1: First order discretization of the river bottom. Due to bottom jump at the cell interface, the momentum flux is not continuous.

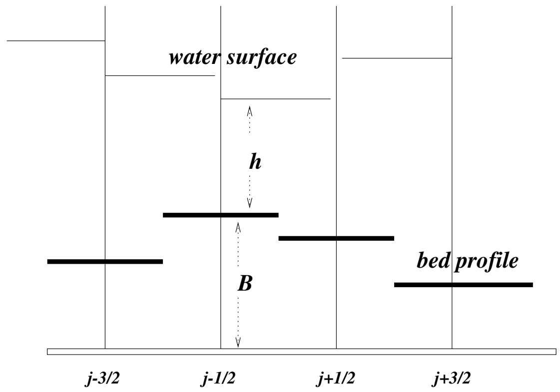

Figure 2: With the shift of the cell interface, the source term effect needs to be accounted for inside each cell.

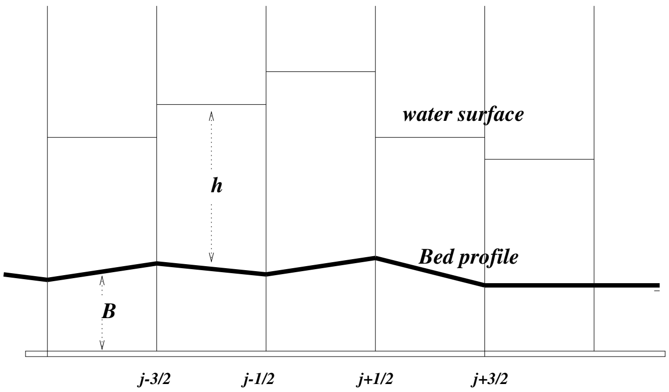

Figure 3: Second-order discretization of the river bottom. The bottom profile inside each cell has a linear distribution.

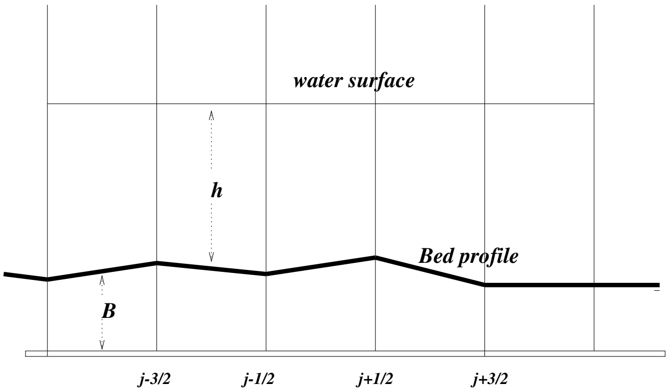

Figure 4: A special solution of the shallow water equations with source term, where $h + B =$ constant and $U = 0$.

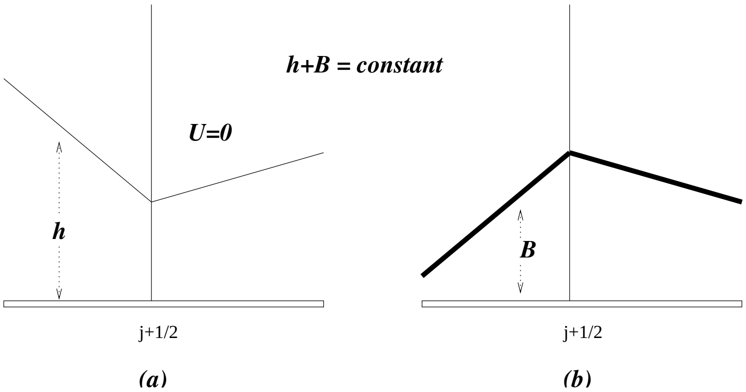

Figure 5: The initial condition of h, U and B around a cell interface for the solution in Fig.(4). For a well balanced scheme, the correct flow evolution in this case should keep a time-independent pressure contribution only at the cell interface.

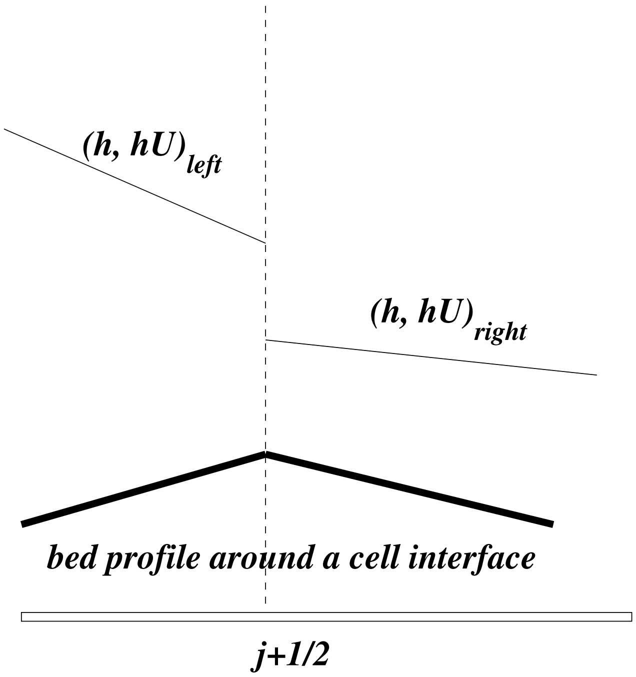

Figure 6: The initial condition for the gas-kinetic BGK scheme. A time dependent flux is obtained with the inclusion of both linearly distributed initial flow variables and the river bed slopes.

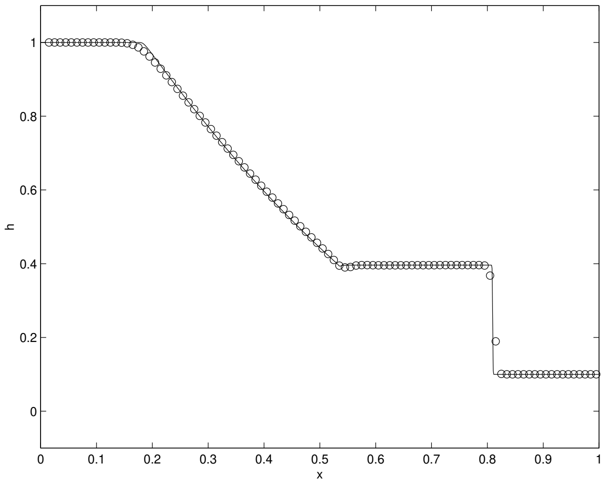

Figure 7: The BGK solution of a shock tube problem with flat river bottom. The homogeneous shallow water equations are solved. Water height is presented and the cell size is $\Delta x = 1/100$.

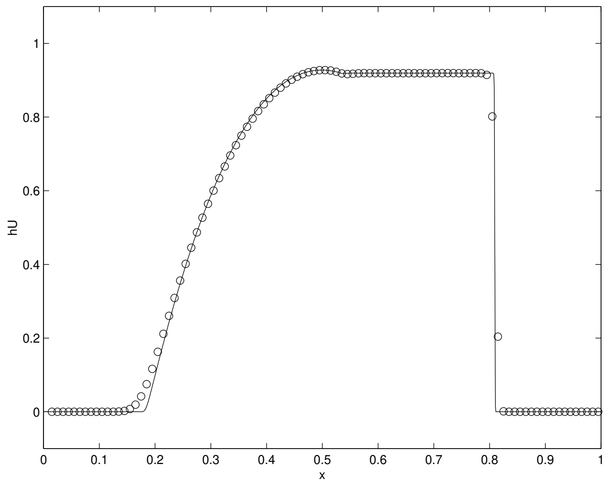

Figure 8: Continuation of Fig.(7). Momentum distribution.

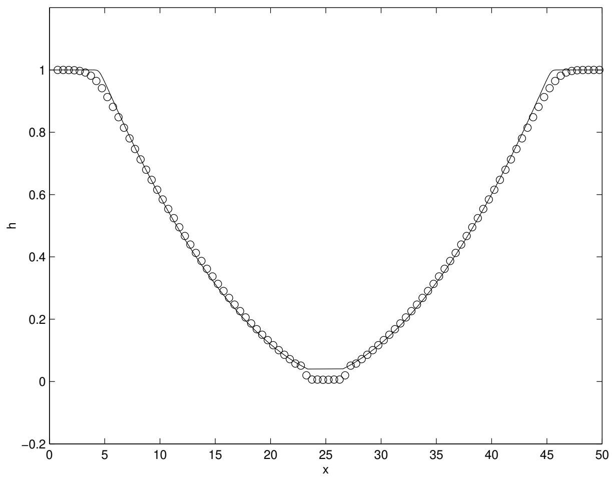

Figure 9: The BGK solution for the shock tube problem with two rarefaction waves. The cell size used is $\Delta x = 0.5$. Water height h is presented and the solid line is the exact solution.

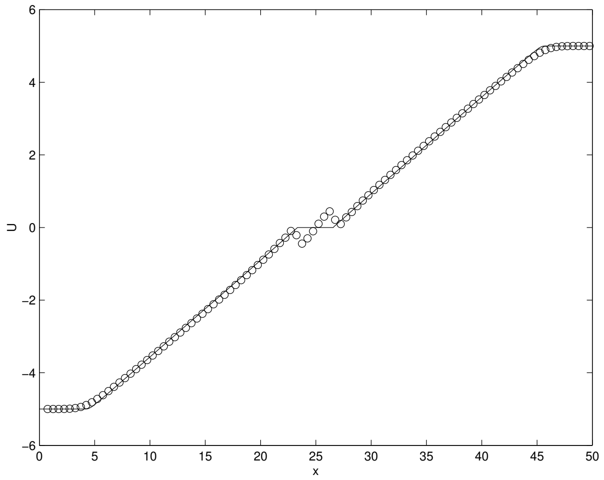

Figure 10: Continuation of Fig.(9). Velocity distribution.

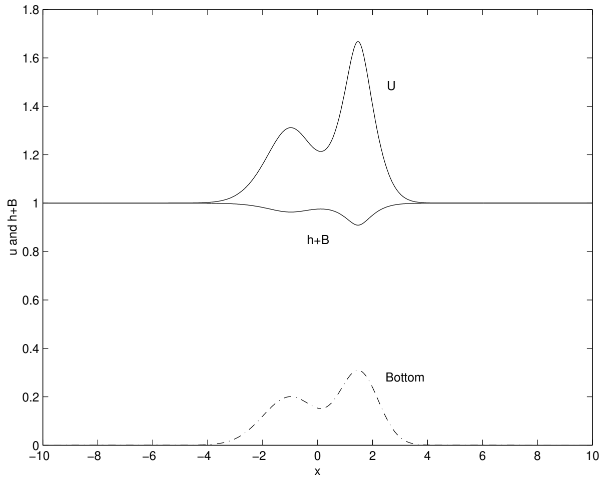

Figure 11: River bottom and exact steady state solution for Case(2).

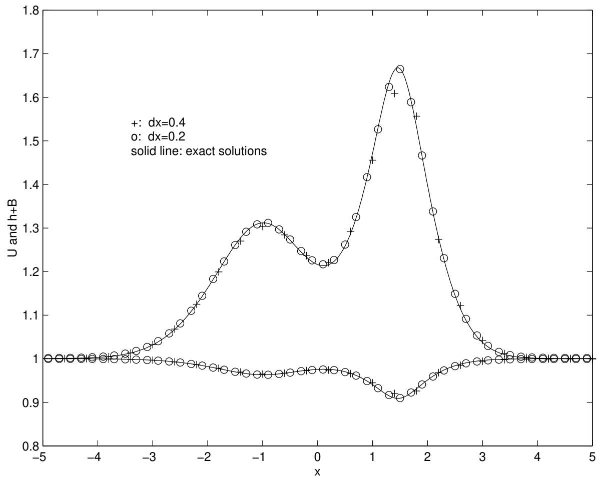

Figure 12: The numerical solutions (U and $h + B$) of Case(2), where 100 (o) and 50 (+) grid points are used in the computational domain $x \in [-10, 10]$. The solid lines are exact solutions. The plot domain is $x \in [-5, 5]$.

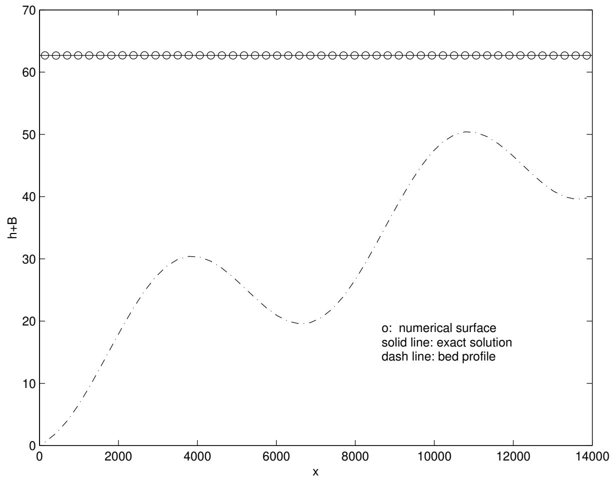

Figure 13: Water surface and river bottom distributions for Case(3). The circles are numerical solution calculated with 50 grid points and the solid line is the exact solution.

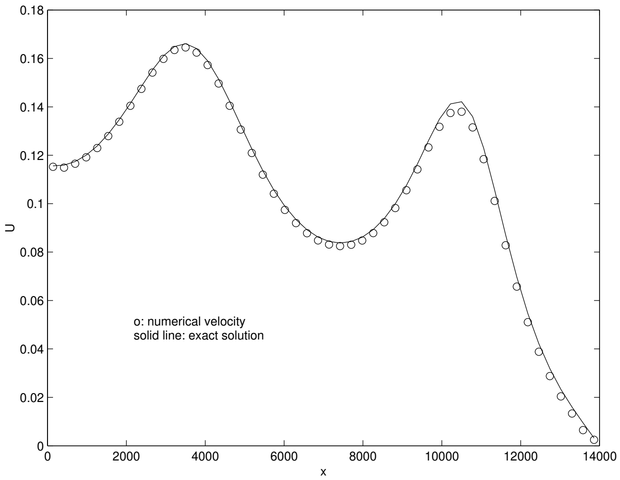

Figure 14: Velocity distribution at time $t = 7552.13s$. 50 grid points are used in the calculation and the solid line is the analytic solution.

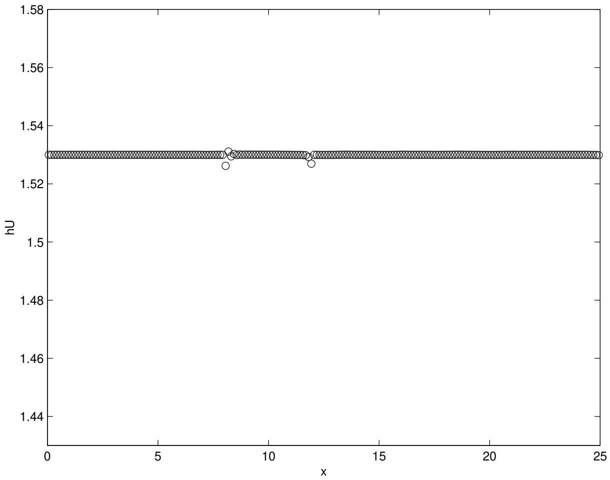

Figure 15: Transcritical flow without a shock. Flow discharge hU is plotted and the exact solution is $hU = 1.53m^2/s$. 200 grid points are used in this case.

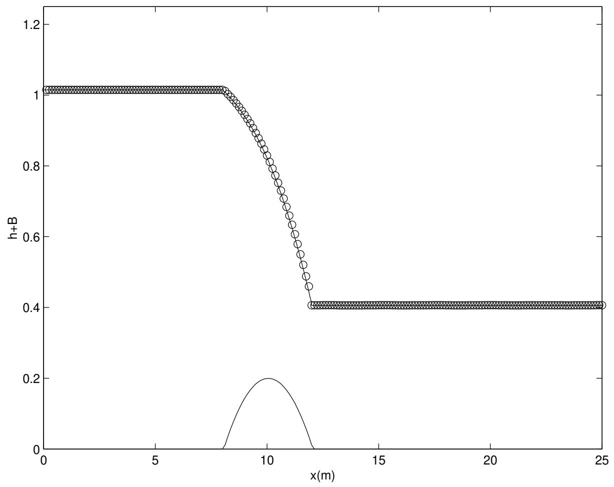

Figure 16: Continuation of Fig.(15). Water surface height $h + B$.

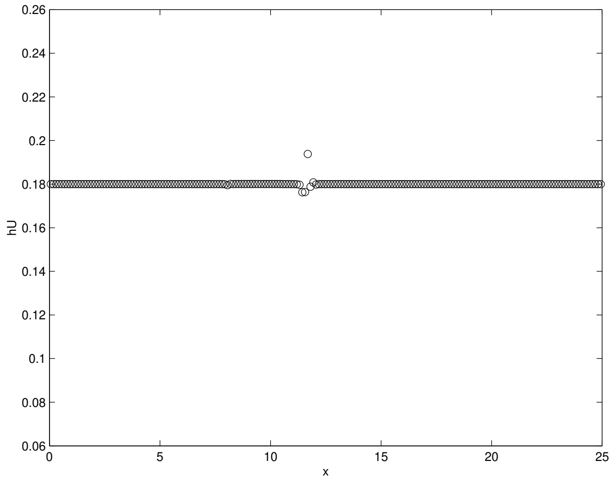

Figure 17: Flow discharge hU in transcritical flow with a shock case. The exact solution is $hU = 0.18$. 200 grid points are used in the calculation.

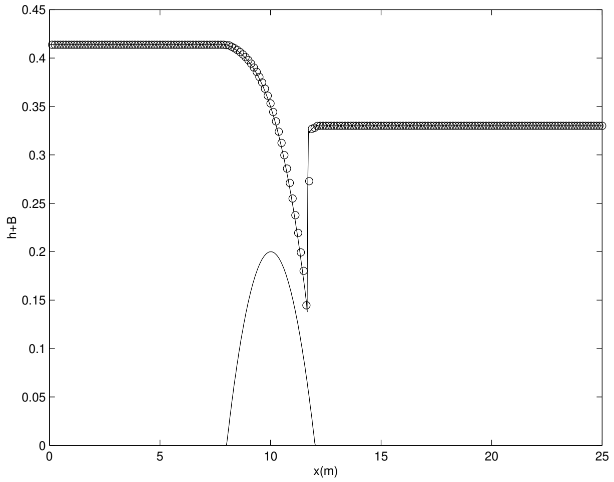

Figure 18: Continuation of Fig.(17). Water surface distribution $h + B$.

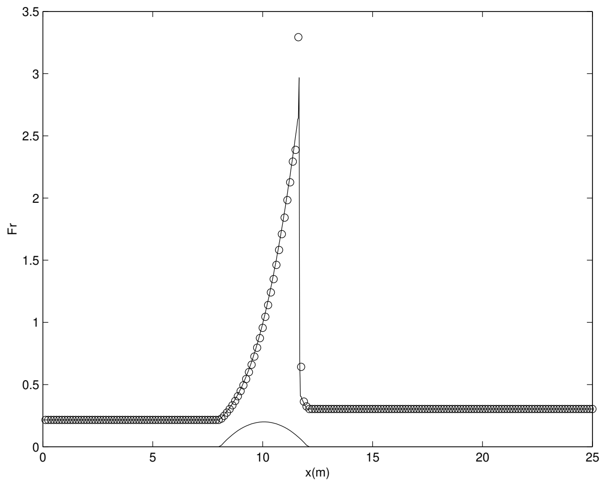

Figure 19: Continuation of Fig.(17). Froude number $U/\sqrt{Gh}$ distribution.

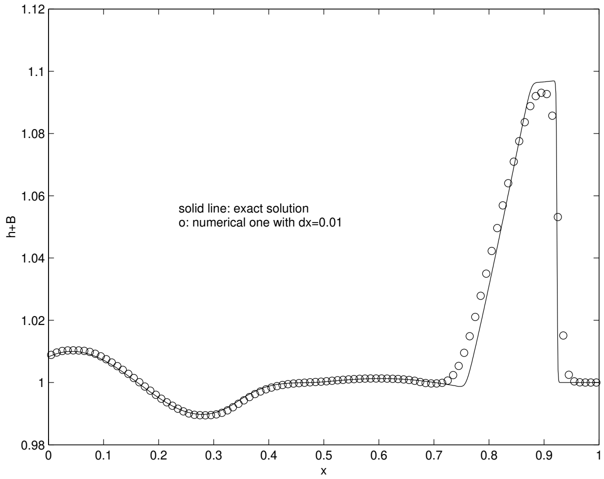

Figure 20: Water height $h + B$ distribution in LeVeque's case with $\epsilon = 0.2$ and the output time is $t = 0.7$. 100 grid points are used in the calculation. The solid line is the numerical solution obtained with 1000 grid points.

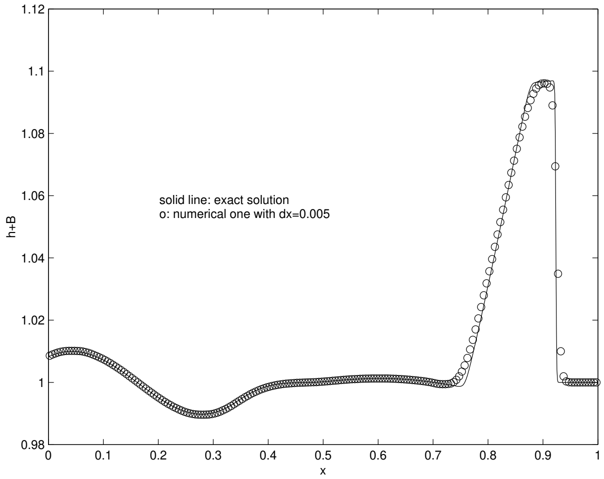

Figure 21: Continuation of Fig.(20). 200 grid points are used.

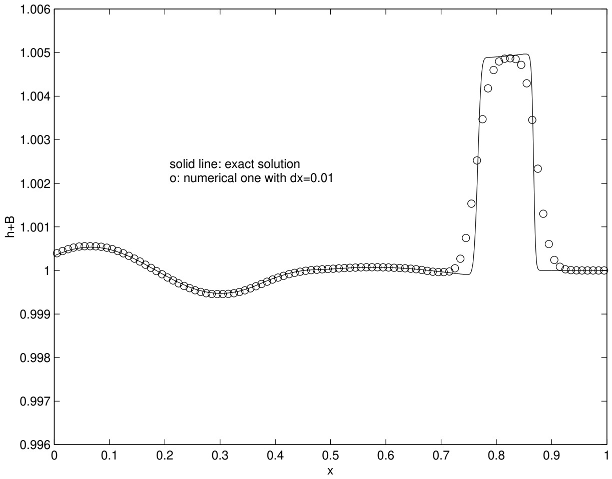

Figure 22: Water height $h + B$ distribution in LeVeque's case with $\epsilon = 0.01$. The output time is $t = 0.7$. 100 grid points are used. The solid line is the numerical solution obtained with 1000 grid points.

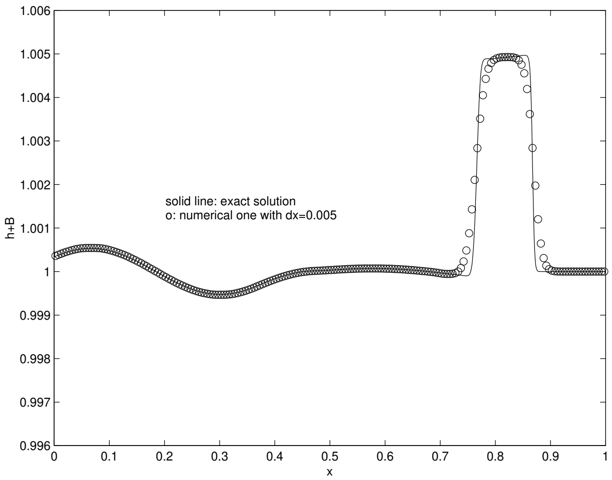

Figure 23: Continuation of Fig.(22). 200 grid points are used.